

PSO-embedded adaptive Kriging surrogate model method for reliability analysis with small failure probability

Wenxiong Li*, Rong Geng, Suiyin Chen

College of Water Conservancy and Civil Engineering, South China Agricultural University, Guangzhou
510642, China

*Corresponding author. E-mail: leewenxiong@scau.edu.cn

Abstract This study introduces a novel adaptive surrogate model methodology for the reliability analysis of systems exhibiting small failure probabilities. To circumvent the limitations inherent in conventional adaptive Kriging surrogate model methodologies reliant on candidate sample pools, an adaptive Kriging surrogate model methodology incorporating the Particle Swarm Optimization (PSO) algorithm is proposed. During implementation, the surrogate model is iteratively refined and high-value samples are selected to update the surrogate model through an optimization solution facilitated by PSO. Meanwhile, two modified learning functions that account for local neighborhood effects and distribution distance of samples for experimental design are introduced to achieve an optimal balance between solution accuracy and efficiency for the proposed methodology. The computational performance of the proposed methodology is assessed using numerical examples. The results indicate that the integration of PSO not only enhances the probability of obtaining high-value samples but also markedly improves the solution accuracy of the adaptive Kriging surrogate model methodology for reliability analysis. By leveraging an optimization algorithm to determine high-value samples, the proposed methodology transcends the limitations of conventional candidate pool-based selection methods, exhibiting exceptional performance in addressing small failure probabilities.

Keywords Structural reliability; Kriging model; Particle swarm optimization algorithm; Adaptive surrogate model; Learning function

1. Introduction

Engineering systems are subject to a multitude of uncertain factors that can significantly impact their reliability and safety. The presence of uncertainties exposes the engineering system to the risk of failure, potentially resulting in severe consequences, including loss of life and property. Consequently, reliability analysis has garnered considerable attention in diverse engineering domains such as mechanical systems [1], infrastructure engineering [2], automotive [3], and

industrial robotics [4].

Over the past several decades, a plethora of reliability methodologies have been proposed. The First Order Reliability Method (FORM) and the Second Order Reliability Method (SORM) represent classical approaches to conducting system reliability analysis. These methodologies entail first-order and second-order Taylor expansions of the performance function, with the Most Probable Points (MPP) and value of the reliability index determined iteratively. However, due to the omission of high-order terms in the expansion, the solution precision of FORM and SORM is relatively low, rendering them unsuitable for addressing problems with highly nonlinear performance functions. Monte Carlo Simulation (MCS) [5, 8] can be employed to ascertain the failure probability of components or systems through random simulation and statistical testing. This methodology is applicable for addressing a wide range of reliability problems with highly nonlinear and complex performance functions. Nevertheless, crude Monte Carlo simulation typically necessitates a large number of random samples and numerical simulations (such as finite element analysis) to determine the value of the performance function for each sample. This results in a significant time cost for reliability analysis. Consequently, crude Monte Carlo simulation is often utilized as a benchmark to gauge the merits and demerits of other methodologies but is challenging to directly apply to engineering works. In recent years, surrogate model methodologies [9, 10] have emerged as a novel solution for system reliability analysis. These methodologies generally involve two steps: first, constructing a surrogate model to approximate the performance function based on Design of Experiment (DoE) data, which encompasses sample points for system uncertainties and corresponding performance function values; second, performing Monte Carlo simulation using the established surrogate model in lieu of the real performance function to calculate the system's failure probability. Unlike crude MCS, surrogate model methodologies can achieve significantly higher efficiency as repeated numerical simulations are not required to determine the values of performance functions. Commonly employed surrogate models include polynomial response surface models [11, 12], radial basis function models [13], Kriging models [14, 53], neural network models [15], support vector machine models [16, 17], and their combination models. The accuracy of the surrogate model is intimately linked to DoE data. Two points warrant consideration when selecting data for DoE. First, high-value samples are conducive to establishing high-precision surrogate models. In other words, when equivalent levels of accuracy are required, the scale of DoE for constructing the surrogate model can be reduced by utilizing high-value samples. Second, as the scale of DoE increases, so does the computational workload and time cost required to establish the surrogate model. Conventional approaches to generating DoE data based on random sampling often fail to select high-value sample points and it can be challenging to determine the appropriate scale

of DoE. As a result, the applicability of surrogate model methodologies is impacted. To address these challenges, adaptive surrogate model methodologies developed in recent years have provided a novel solution for reliability analysis.

The primary distinction between adaptive surrogate model methodologies and conventional surrogate model methodologies resides in the selection of samples for DoE. In adaptive methodologies, the surrogate model is established through incremental refinement, with a learning function typically employed to guide the selection of high-value samples for DoE during model construction. In recent years, scholars have extensively debated the implementation and performance of adaptive methodologies based on various surrogate models, including support vector machine models [20, 21], radial basis function models [22, 23], neural network models [24-27], and Kriging models [28, 29]. Due to its precise interpolation and effective estimation of uncertainty, the Kriging model is commonly utilized to establish adaptive surrogate model methodologies. Echard et al. [30] proposed an adaptive surrogate model methodology based on the Kriging model, denoted as AK-MCS. In this methodology, the learning function for a candidate point is determined based on the mean value and Kriging variance of its performance function. Faurat and Gayton [31] introduced the AK-SYS methodology by integrating AK-MCS with Efficient Global Reliability Analysis (EGRA) to analyze system reliability with multiple failure modes. Zhang et al. [39] employed the Reliability Expectation Improvement Function (REIF) to develop an active learning surrogate model methodology. Yun et al. [40] proposed an adaptive Kriging surrogate model methodology based on a modified U learning function for system reliability analysis of problems with multiple failure modes. Xiao et al. [29] introduced an adaptive Kriging surrogate model methodology with a novel learning function based on cross-validation that accounts for both the epistemic uncertainty of surrogate models and the aleatory uncertainty of random variables. Xiao et al. [41] further explored the adaptive Kriging surrogate model methodology by considering multiple failure modes and mixed variables. Ma et al. [28] conducted a comparative study on the impact of initial DoE data, learning functions, and stopping criteria on the solution performance of an adaptive Kriging surrogate model methodology.

Within the framework of AK-MCS, high-value samples required for updating the surrogate model are typically obtained using a selection strategy based on the Candidate Sample Pool (CSP). To estimate small failure probabilities, a large-scale CSP is necessary to obtain a robust and convergent failure probability estimate. During the process of updating the Kriging model, the AK-MCS methodology must estimate the learning function value for all samples in CSP to iteratively select a new training sample to update the Kriging model. This process is time-consuming and reduces the efficiency of the AK-MCS methodology for estimating small

failure probabilities. To enhance the efficiency of the AK-MCS methodology for estimating small failure probability, numerous improved AK-MCS methodologies have been proposed. Echard et al. [32] proposed the AK-IS methodology by combining AK-MCS with an importance sampling methodology. Balesdent et al. [33] and Zhao et al. [34] conducted research on the combination of an adaptive Kriging surrogate model and importance sampling methodology. Yun et al. [35] proposed the AK-MIS methodology that combines an adaptive Kriging surrogate model and modified importance sampling to further distinguish important regions from unimportant ones based on AK-IS, with a Kriging surrogate model constructed in the important regions. Sun et al. [36] presented an adaptive Kriging surrogate model methodology based on the Least Improved Function (LIF), which combines Markov Chain Monte Carlo simulation (MCMC) to address problems with nonlinear performance functions and small failure probabilities. Building on AK-MCS and K-weighted-means clustering, Lelièvre et al. [37] introduced multipoint enhancement technology and developed AK-MC*S*i for reliability analysis. Lv et al. [38] proposed a novel learning function based on information entropy for the Kriging methodology and introduced the AK-LS methodology, which combines active learning Kriging model with line sampling, to ensure the reliability of complex structures with small failure probability and multidimensional variables. Xiao et al. [29] developed an adaptive Kriging surrogate model methodology by introducing adaptive importance sampling. Zhou et al. [42] introduced an adaptive Kriging surrogate model methodology that employs a point selection strategy with a limited region, defined as the region that significantly contributes to the accuracy of the surrogate model. Xu et al. [54] proposed a modified algorithm that combines AK-MCS and modified subset simulation to estimate small failure probabilities. Yun et al. [55] presented an improved AK-MCS based on adaptive radial-based importance sampling used to reduce the number of candidate points in the AK-MCS methodology. Liu et al. [56] developed an enhanced AK-MCS by utilizing an efficient CSP reduction strategy.

The improvements to AK-MCS methods mentioned above generally aim to reduce the size of CSP while ensuring accurate and robust estimation of failure probability. These methods primarily achieve this reduction through advanced sampling techniques or important region selection, thereby improving the efficiency of constructing a Kriging model for the actual performance function. However, there are limitations to their application compared to direct MCS. For example, the MPP is required, which presents challenges for problems with multiple MPPs. Additionally, subset simulation used in AK-MCS requires generating conditional samples through Markov Chain Monte Carlo simulation and approximating the performance function corresponding to each intermediate failure event. The total number of model evaluations for these methods may be larger than that of the AK-MCS method. The determination of high-value points in AK-MCS is essentially an

optimization problem. According to the literature review presented, no article provides a specific implementation of an optimization method for selecting high-value points in AK-MCS and discusses the appropriate setting of the learning function related to the optimization algorithm. To address the limitations of adaptive Kriging surrogate model methods based on CSP, this paper proposes a novel adaptive surrogate model method based on an optimization algorithm for reliability analysis with small failure probabilities. In this approach, the Particle Swarm Optimization (PSO) algorithm [43, 44] is integrated into the framework of AK-MCS. The surrogate model is then iteratively improved according to high-value samples selected through an optimization solution using PSO during implementation, avoiding the compute-intensive workload of evaluating a large number of candidate samples.

2. AK-MCS

This section introduces the Adaptive Kriging surrogate model-based Monte Carlo Simulation method (AK-MCS) [28, 30, 31, 37]. Firstly, the specific form of the Kriging model used in AKMCS is presented. Then, the principles and implementation of AK-MCS for reliability analysis are introduced.

2.1. Kriging model

Kriging model is a nonlinear interpolation meta-model developed for geostatistics. In system reliability analysis, Kriging model can be used as a surrogate model to approximate the relationship between system input and output, such as the relationship between the sampling points and the performance function values corresponding to these sampling points. Generally, Kriging model consists of two parts, i.e. a parametric linear regression model and a nonparametric stochastic process. The approximate relationship between any experiment $\mathbf{x} = (x_1, x_2, \dots, x_n)^T$ and the response $\hat{G}(\mathbf{x})$ can be denoted as [30]

$$\hat{G}(\mathbf{x}) = \mathbf{f}^T(\mathbf{x})\boldsymbol{\beta} + z(\mathbf{x}) \quad (1)$$

where $\mathbf{f}^T(\mathbf{x})\boldsymbol{\beta}$ represents the deterministic part which gives an approximation of the response in mean, $\mathbf{f}^T(\mathbf{x}) = \{f_1(\mathbf{x}), f_2(\mathbf{x}), \dots, f_k(\mathbf{x})\}$ represents the basis functions and $\boldsymbol{\beta}^T = \{\beta_1, \beta_2, \dots, \beta_k\}$ is the vector of regression coefficients. In this paper, ordinary Kriging model is selected which means that $f_i(\mathbf{x}) = 1$ ($i = 1, 2, \dots, k$). In Eq.(1), $z(\mathbf{x})$ is a stationary Gaussian process with zero mean $z(\mathbf{x}) \sim N(0, \sigma^2)$, and the covariance between two points of space \mathbf{x}^i and \mathbf{x}^j is defined as

$$\text{Cov}[z(\mathbf{x}^i), z(\mathbf{x}^j)] = \sigma^2 R(\boldsymbol{\theta}, \mathbf{x}^i, \mathbf{x}^j) \quad (2)$$

where σ^2 is the process variance, $\boldsymbol{\theta} = \{\theta_1, \theta_2, \dots, \theta_n\}$ refers to the parameter vector, and $R(\boldsymbol{\theta}, \mathbf{x}^i, \mathbf{x}^j)$ represents the correlation function between \mathbf{x}^i and \mathbf{x}^j , which is formulated by

$$R(\boldsymbol{\theta}, \mathbf{x}^i, \mathbf{x}^j) = \exp \left[- \sum_{d=1}^n \theta_d (x_d^i - x_d^j)^2 \right] \quad (3)$$

where x_d^i and x_d^j refers to the d^{th} component in \mathbf{x}^i and \mathbf{x}^j , respectively.

Given the sample set of DoE $\mathbf{S}_{\text{DoE}} = [\mathbf{x}^1, \mathbf{x}^2, \dots, \mathbf{x}^m]$ and the corresponding response set $\mathbf{Y}_{\text{DoE}} = [G(\mathbf{x}^1), G(\mathbf{x}^2), \dots, G(\mathbf{x}^m)]$ with m being the number of samples in DoE, the scalars β and σ^2 are estimated by [30]

$$\hat{\beta} = (\mathbf{1}^T \mathbf{R}^{-1} \mathbf{1})^{-1} \mathbf{R}^{-1} \mathbf{Y}_{\text{DoE}} \quad (4)$$

$$\hat{\sigma}^2 = \frac{1}{m} (\mathbf{Y}_{\text{DoE}} - \hat{\beta} \mathbf{1})^T \mathbf{R}^{-1} (\mathbf{Y}_{\text{DoE}} - \hat{\beta} \mathbf{1}) \quad (5)$$

where \mathbf{R} is the correlation matrix with the component $R_{i,j} = R(\boldsymbol{\theta}, \mathbf{x}^i, \mathbf{x}^j)$ in which represents the correlation between each pair of points in DoE, and $\mathbf{1}$ refers to the vector filled with 1 of length m . $\hat{\beta}$ and $\hat{\sigma}^2$ in Eqs. (4) and (5) are related to the correlation parameters θ_i through the matrix \mathbf{R} , then the value of $\boldsymbol{\theta}$ is required to be firstly obtained by using maximum likelihood estimation:

$$\boldsymbol{\theta} = \arg \min_{\boldsymbol{\theta}} (\det(\mathbf{R}))^{\frac{1}{m}} \hat{\sigma}^2 \quad (6)$$

According to the Gaussian process regression theory, the system response follows the normal distribution as $G(\mathbf{x}) \sim N(\mu_G(\mathbf{x}), \sigma_G(\mathbf{x}))$. Then, based on the Kriging model established according to the given data of DoE, the Best Linear Unbiased Predictor (BLUP) of the response $\hat{G}(\mathbf{x})$ at an unknown point \mathbf{x} is shown to be a Gaussian random variate $\hat{G}(\mathbf{x}) \sim N(\mu_{\hat{G}}(\mathbf{x}), \sigma_{\hat{G}}(\mathbf{x}))$ where

$$\mu_{\hat{G}}(\mathbf{x}) = \hat{\beta} + \mathbf{r}(\mathbf{x}) \mathbf{R}^{-1} (\mathbf{Y}_{\text{DoE}} - \hat{\beta} \mathbf{1}) \quad (7)$$

$$\sigma_{\hat{G}}^2(\mathbf{x}) = \hat{\sigma}^2 \left(\mathbf{1} - \mathbf{r}^T(\mathbf{x}) \mathbf{R}^{-1} \mathbf{r}(\mathbf{x}) + u^T(\mathbf{x}) (\mathbf{1}^T \mathbf{R}^{-1} \mathbf{1})^{-1} u(\mathbf{x}) \right) \quad (8)$$

where $\mathbf{r}(\mathbf{x}) = [R(\boldsymbol{\theta}, \mathbf{x}, \mathbf{x}^1), R(\boldsymbol{\theta}, \mathbf{x}, \mathbf{x}^2), \dots, R(\boldsymbol{\theta}, \mathbf{x}, \mathbf{x}^m)]^T$ and $u(\mathbf{x}) = \mathbf{1}^T \mathbf{R}^{-1} \mathbf{r}(\mathbf{x}) - 1$.

In Kriging model, the predicted mean value at any point \mathbf{x}^i in DoE is consistent with the true response value, namely $\mu_{\hat{G}}(\mathbf{x}^i) = G(\mathbf{x}^i) (i=1, 2, \dots, m)$, and the corresponding Kriging variance is null, namely $\sigma_{\hat{G}}^2(\mathbf{x}^i) = 0 (i=1, 2, \dots, m)$. For any point out of DoE, the Kriging variance is not zero,

and its value reflects the accuracy of the prediction results at the point. For clarity, **Fig. 1** demonstrates an example of prediction results of Kriging model within the range of $[0,10.0]$, which include $\mu_{\hat{G}}(x)(x \in [0,10.0])$ and $\mu_{\hat{G}} \pm \sigma_{\hat{G}}(x)(x \in [0,10.0])$, based on the given sample data in DoE. The Kriging variance of Kriging model provides a basis for selecting high-value experimental design points. Generally, learning functions can be constructed according to Kriging variance and predicted mean value to realize active learning based on the current Kriging model, and finally the perfect Kriging model can be established.

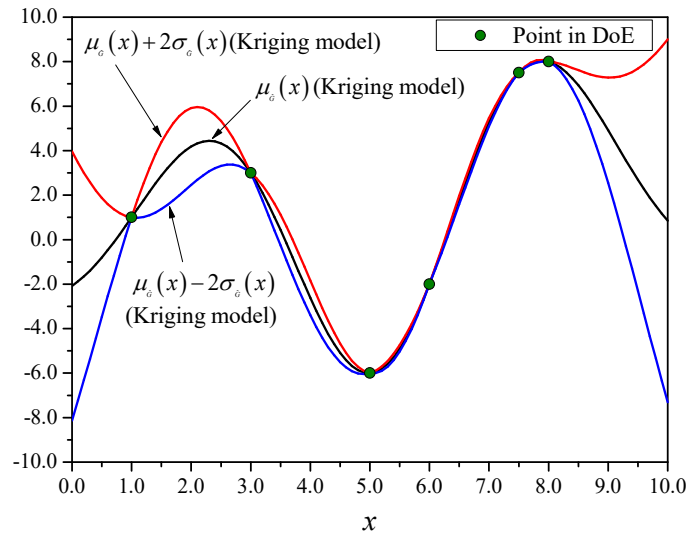


Fig. 1. The predicted mean value and Kriging variance of Kriging model.

2.2. Implementation of AK-MCS

The Kriging model, based on the given data from the Design of Experiments (DoE), approximates the relationship between sample points and performance function values, and predicts the shape of the limit state surface. By using the established Kriging model as a surrogate model, the failure probability can be determined through Monte Carlo simulation using the following formula:

$$\hat{P}_f = \frac{n_{\hat{G} \leq 0}}{n_{MC}} \quad (9)$$

where n_{MC} represents the total number of sampling in MCS and $n_{\hat{G} \leq 0}$ refers to number of sampling with $\hat{G} \leq 0$ in MCS.

To address the issue of constructing data for DoE, scholars have proposed the adaptive Kriging surrogate model with active learning ability and the AK-MCS [28, 30, 31, 37] by combining the adaptive surrogate model with Monte Carlo simulation. This approach involves gradually

improving the Kriging model through a series of iterative processes. In each iteration, all candidate samples are evaluated using the current Kriging model with a predefined learning function. The sample with the highest (or lowest) value of the learning function is selected and added to DoE for updating the Kriging model. Generally, high-value samples contribute more to improving the accuracy of the Kriging model and typically have the following spatial distribution characteristics: (1) high-value samples are usually close to the limit state surface; and (2) new high-value samples are commonly located in regions where existing DoE samples are relatively sparse due to higher uncertainty.

The learning function is the basis for selecting high-value samples. Various learning functions have been developed, including the sign indication learning function (U function) [30], the Expected Feasibility Function (EFF) [45], the information entropy theory-based learning function (H function) [38], and the Least Improvement Function (LIF) [36]. In this paper, the sign indication learning function (U function) is used to guide the selection of high-value samples. The U function is constructed based on the risk of crossing the limit state surface and is defined as follows:

$$U(\mathbf{x}) = \frac{|\mu_{\hat{G}}(\mathbf{x})|}{\sigma_{\hat{G}}(\mathbf{x})} \quad (10)$$

According to the definition of the U function, samples with a high probability of crossing the limit state surface are added to the DoE set because the positive and negative signs of their corresponding performance function values are easily influenced by uncertain factors, resulting in changes in failure probability. Therefore, high-value samples should be located according to the following conditions: (1) the predicted mean value of the performance function is close to zero; and (2) the Kriging variance of the performance function is relatively high.

In the process of updating the Kriging model, the values of U function for all candidate samples in CSP $\mathbf{S}_{pool} = (\mathbf{x}_c^1, \mathbf{x}_c^2, \dots, \mathbf{x}_c^p)$ are firstly calculated by using the current Kriging model, and then the sample with lowest U value among these candidate samples is added to the set of DoE. Hence, the learning criterion is defined as $\min(U(\mathbf{x}))(\mathbf{x} \in \mathbf{S}_{pool})$.

In AK-MCS proposed by Echard et al. [30], the stop condition of Kriging model update process is set to be $\min(U(\mathbf{x})) \geq 2.0$ [30]. It is considered that the correct rate of the surrogate model's response signs to the Monte Carlo population can be guaranteed if the stop condition is met. Considering there may still be deviation between the predicted response value using the surrogate model and the real response value, because the samples of DoE used to generate the surrogate model may be insufficient, which makes the surrogate model unable to accurately depict the

characteristics of the limit state surface. Therefore, the variation coefficient of failure probability $V_{\hat{P}_f}$ expressed as follows should be further accessed

$$V_{\hat{P}_f} = \sqrt{(1 - \hat{P}_f) / (\hat{P}_f n_{MC})} \quad (11)$$

When $V_{\hat{P}_f}$ exceeds the preset limit value, it is considered that the scale of the current Monte Carlo population is not large enough, and the number of sampling points in Monte Carlo simulation should be increased. It should be noted that in AK-MCS, the Monte Carlo population is also used as the pool of candidate samples, so the scale of the candidate pool increases accordingly. Correspondingly, the set of DoE and Kriging surrogate model are continuously updated.

Reference [30] provides details on the implementation of AK-MCS. Since high-value samples are selected from CSP, the distribution of candidate samples significantly impacts the acquisition of high-value samples. Candidate samples are obtained through Monte Carlo sampling according to the distribution parameters of random variables and generally follow a standard normal distribution. However, the distribution of candidate samples in the edge regions of Monte Carlo sampling is relatively sparse, making it difficult to obtain real high-value samples for these regions. Considering that reliability analysis for practical engineering often involves small failure probabilities, where real high-value sample points often exist at the sampling edge, large-scale candidate pools are required to ensure that real high-value sample points can be found. Additionally, for problems with small failure probabilities, a large-scale Monte Carlo population is required to meet the limit condition of the variation coefficient of failure probability. In other words, as failure probability decreases, the scale of the Monte Carlo population and candidate pool increases accordingly. It is worth noting that as the scale of the candidate pool increases, so does the computational effort required to evaluate candidate samples using the Kriging surrogate model, ultimately affecting the efficiency of adaptive Kriging surrogate model methods. Therefore, overcoming the limitations of candidate pool-based methods in selecting high-value samples is key for adaptive Kriging surrogate model methods to solve reliability analysis problems with small failure probabilities. The authors believe that using an optimization algorithm to obtain high-value samples, rather than the conventional CSP-based method, is a promising approach to improving the performance of adaptive Kriging surrogate model methods.

3. PSO-AK-MCS

In the selection of high-value samples, the objective is to minimize the value of the function defined in Eq. (10) within a given design space. The values of random variables are treated as design variables. The learning function is often a complex, nonlinear function with multiple peaks

(or valleys). Conventional optimization algorithms, such as gradient-based methods, may only yield local optima and produce suboptimal results. In contrast, modern optimization algorithms such as Genetic Algorithm (GA), Ant Colony Algorithm (ACA), and Particle Swarm Optimization (PSO) are powerful tools for solving optimization problems. These algorithms are theoretically capable of finding global optima and do not require the optimized functions to be differentiable or continuous. Given its effectiveness in handling continuous variable optimization and ease of implementation, PSO is employed as the primary algorithm for optimization in this work.

In this work, a PSO-embedded Adaptive Kriging surrogate model-based Monte Carlo Simulation method (PSO-AK-MCS) is proposed for reliability analysis. In this approach, high-value samples are selected by PSO. As the selection process for high-value samples is no longer dependent on the scale of CSP or the distribution characteristics of random variables, the likelihood of obtaining high-value samples is significantly increased.

3.1. Implementation of PSO

PSO was originally introduced by Kennedy and Eberhart in 1995 [46]. The algorithm is designed to solve global optimization problems involving nonlinear objective functions with continuous variables. The underlying concept of PSO is inspired by the foraging behavior of birds, where individuals follow the best-performing member of the flock without knowing the exact location or distance to food. In PSO, each potential solution to the optimization problem is represented as a ‘particle’ in the search space. Particles are evaluated based on a fitness function determined by the objective function and move through the solution space at random speeds. Through information exchange, particles can obtain heuristic information to guide the swarm towards an optimal solution. PSO has been applied in various fields, including structural optimization [47], topology optimization [48], structural reliability evaluation [49], complex network reliability optimization [50], and reliability optimization design [51]. For further developments and applications of PSO, readers are referred to Ref. [43].

An optimization problem with a N_D -dimension search space can be solved by using PSO with the size of particle swarm (number of particles) N_{swarm} and the maximum iteration number N_{ite_max} predetermined. When the algorithm runs to the n^{th} ($n=1,2,\dots,N_{ite_max}$) iteration, the current position and current velocity of the i^{th} ($i=1,2,\dots,N_{swarm}$) particle are expressed as $\mathbf{X}_i^{(n)} = (X_{i,1}^{(n)}, X_{i,2}^{(n)}, \dots, X_{i,N_D}^{(n)})$ and $\mathbf{V}_i^{(n)} = (V_{i,1}^{(n)}, V_{i,2}^{(n)}, \dots, V_{i,N_D}^{(n)})$, respectively. Then, for each particle, the following formulas are used to update the speed and position in each dimension component at each iteration [43, 49].

$$V_{i,j}^{(n+1)} = \omega \cdot V_{i,j}^{(n)} + c_1 \cdot rand \cdot (X_{pbest,i,j}^{(n)} - X_{i,j}^{(n)}) + c_2 \cdot rand \cdot (X_{gbest,j}^{(n)} - X_{i,j}^{(n)}) \quad (j = 1, 2, \dots, N_D) \quad (12)$$

$$X_{i,j}^{(n+1)} = X_{i,j}^{(n)} + V_{i,j}^{(n+1)} \quad (j = 1, 2, \dots, N_D) \quad (13)$$

In Eq. (12), ω is the inertia weight, c_1 and c_2 refer to the cognition learning factor and social learning factor, respectively, $X_{pbest,i,j}^{(n)}$ represents the j^{th} component of the historical best position of the i^{th} particle at the n^{th} iteration, $X_{gbest,j}^{(n)}$ represents the j^{th} component of the best position of the whole swarm at the n iteration, $rand$ means to generate a random value uniformly distributed within the range of $[0,1]$. For the sake of convenience, the historical best position of a particle and the best position of the whole swarm at the n^{th} iteration are expressed as

$$\mathbf{X}_{pbest,i}^{(n)} = (X_{pbest,i,1}^{(n)}, X_{pbest,i,2}^{(n)}, \dots, X_{pbest,i,N_D}^{(n)}) \quad \text{and} \quad \mathbf{X}_{gbest}^{(n)} = (X_{gbest,1}^{(n)}, X_{gbest,2}^{(n)}, \dots, X_{gbest,N_D}^{(n)}), \quad \text{respectively.}$$

Generally, the historical best position of a particle $\mathbf{X}_{pbest,i}^{(n)}$ changes with the iteration process and can be described by

$$\mathbf{X}_{pbest,i}^{(n+1)} = \begin{cases} \mathbf{X}_i^{(n+1)}, & \text{if } F_{\text{fit}}(\mathbf{X}_i^{(n+1)}) < F_{\text{fit}}(\mathbf{X}_{pbest,i}^{(n)}) \\ \mathbf{X}_{pbest,i}^{(n)}, & \text{otherwise} \end{cases} \quad (14)$$

where $F_{\text{fit}}(\cdot)$ refers to the fitness function. Among the historical best positions of all particles, the best position with the highest fitness value is recorded as the best position of the whole swarm, expressed as

$$\begin{aligned} \mathbf{X}_{gbest}^{(n)} &\in \left\{ \mathbf{X}_{pbest,1}^{(n)}, \mathbf{X}_{pbest,2}^{(n)}, \dots, \mathbf{X}_{pbest,N_{\text{swarm}}}^{(n)} \mid F_{\text{fit}}(\mathbf{X}_{pbest,i}^{(n)}) \right\} \\ &= \max \left\{ F_{\text{fit}}(\mathbf{X}_{pbest,1}^{(n)}), F_{\text{fit}}(\mathbf{X}_{pbest,2}^{(n)}), \dots, F_{\text{fit}}(\mathbf{X}_{pbest,N_{\text{swarm}}}^{(n)}) \right\} \end{aligned} \quad (15)$$

As discussed above, the movement of particles is influenced by three factors. The first is the current speed of motion, which reflects the continuity of particle movement between successive iterations. The second is the particle's historical best position, which reflects the influence of its own experience on its direction of movement. The third is the best position of the swarm, which reflects the influence of the swarm's collective experience on the direction of particle movement. **Fig. 2** illustrates the motion of a particle.

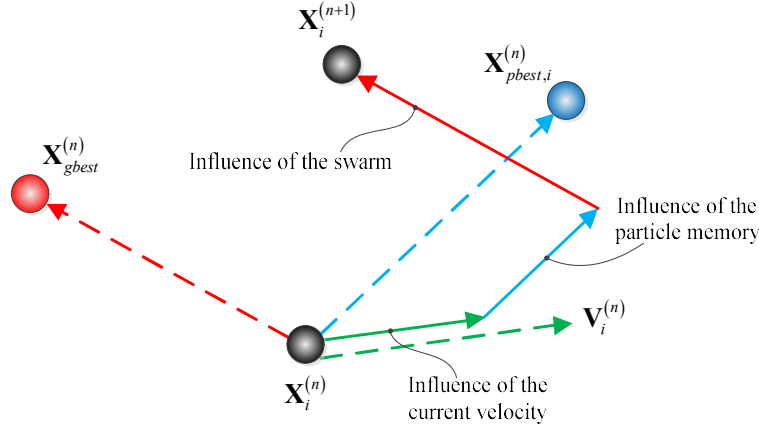


Fig. 2. The sketch map of particle motion in PSO [43].

The performance of PSO is influenced by the parameters ω , c_1 and c_2 . The inertia weight ω is a parameter that controls the influence of a particle's velocity from the previous iteration. Introduced by Shi and Eberhart [49], this parameter affects the balance between global and local search capabilities. A higher inertia weight generally enhances global optimization ability, while a lower inertia weight improves local optimization ability. The value of the inertia weight typically ranges between 0 and 1.0, with a recommended value of 0.729 as suggested by Clerc and Kennedy [52]. Some researchers have also proposed updating strategies that decrease the inertia weight over time. The cognitive learning factor c_1 reflects the influence of the distance between a particle's current position and its historical best position. This means that particles move according to their own cognition. The social learning factor c_2 describes the influence of the distance between a particle's current position and the swarm's best position. This reflects information sharing and cooperation among particles, as well as their tendency to move according to the swarm's collective experience. Both c_1 and c_2 are typically set to 2.0, with a recommended value of 1.494 as suggested by Clerc and Kennedy [52]. Additionally, a velocity limit constant V_{\max} is often introduced to control the maximum distance a particle can move in each iteration, thereby controlling the convergence speed and global search ability of the algorithm.

The main steps of PSO used in this work are as follows.

Step 1: Set control parameters for PSO, including N_{swarm} , $N_{\text{ite_max}}$, ω , c_1 , c_2 and V_{\max} .

Step 2: Initialize the particle swarm by randomly generating the position and velocity of each particle within the solution space. Evaluate all particles in the swarm and set their current position as their historical best position. Determine the swarm's best position according to Eq. (15).

Step 3: Update the position and velocity of all particles using Eqs. (12) and (13). Adjust the

updated particles according to any constraints and generate a new particle swarm.

Step 4: Evaluate all particles in the swarm and determine their historical best position according to Eq. (14). Determine the swarm's best position using Eq. (15).

Step 5: If the maximum number of iterations has been reached, output the swarm's best position and end the program. Otherwise, return to **Step 3** and continue.

3.2. Implementation of PSO-AK-MCS

3.2.1. Optimization model for high-value points

Generally, the values of random variables in the standard normal space are regarded as the design variables and denoted as $\mathbf{X} = (X_1, X_2, \dots, X_{N_D})$. Then, the mathematical model of the optimization for selecting a high-value sample can be expressed as

$$\begin{aligned} \text{find } & \mathbf{X} = (X_1, X_2, \dots, X_{N_D}) \\ \text{min } & F_{\text{obj}}(\mathbf{X}) = U(\mathbf{X}) + p \cdot (\|\mathbf{X}\| - r_c) \\ \text{s.t. } & X_j \in [-X_{\text{lim}}, X_{\text{lim}}] (j = 1, 2, \dots, N_D) \end{aligned} \quad (16)$$

where $X_j (j = 1, 2, \dots, N_D)$ reflects the search range of the j design variable in PSO. Given that the probability of obtaining samples in $(-\infty, -6.0)$ and $(6.0, \infty)$ is extremely small when conducting random sampling according to the standard normal distribution, this paper sets $X_{\text{lim}} = 6.0$. In the implementation of PSO, the fitness function can be obtained by $F_{\text{fit}}(\mathbf{X}) = 1/(F_{\text{obj}}(\mathbf{X}) + \delta)$ with δ the preset small quantity.

In Eq. (16), $F_{\text{obj}}(\mathbf{X})$ represents the objective function, where $U(\mathbf{X})$ is the sign indication learning function (as defined in Eq. (10)) and $p \cdot (\|\mathbf{X}\| - r_c)$ is a penalty term with r_c controlling the sampling range and p representing the penalty intensity, named as penalty coefficient. The purpose of introducing a penalty term is to enable the optimization algorithm to find high-value sample points that are more suitable for constructing high-precision surrogate models. As shown in **Fig. 3**, the edge region of Monte Carlo sampling is actually circular for a problem with two design variables. When calculating failure probability, the contribution of sampling points outside the circular edge to the construction of a high-precision surrogate model typically decreases with increasing distance from the sampling center. Therefore, a hypersphere with a suitable radius r_c can be predefined. For sampling points outside this hypersphere, a penalty term that increases with the magnitude of the sample point can be introduced to reduce the likelihood of selecting such points. For random variables in standard normal space, the value of the probability distribution function at -4.30 is as low as 8.54×10^{-6} . In this work, we set the radius r_c to 4.30, which is

sufficient for most problems involving small failure probabilities. The penalty coefficient p should be set according to the range of performance function values $G(\mathbf{x})$ within the sampling space. In this work, the penalty coefficient is set as follows:

$$p = \frac{\bar{G}(\mathbf{x})|_{\mathbf{x} \in \text{DoE}} - \underline{G}(\mathbf{x})|_{\mathbf{x} \in \text{DoE}}}{4.0} \quad (17)$$

where $\underline{G}(\mathbf{x})|_{\mathbf{x} \in \text{DoE}}$ and $\bar{G}(\mathbf{x})|_{\mathbf{x} \in \text{DoE}}$ represent the minimum and maximum of the performance function values obtained from the current set of DoE. It should be noted that this setting of the penalty coefficient does not strongly restrict high-value sample points to within the specified hypersphere. As long as the objective function value is low enough, samples outside the hypersphere can also be selected as high-value points, avoiding the potential lack of truly high-value sample points due to the limitations of the hypersphere. In fact, for problems involving small failure probabilities, sample points near the hypersphere are also near the limit state surface and play an important role in calculating failure probability using surrogate models.

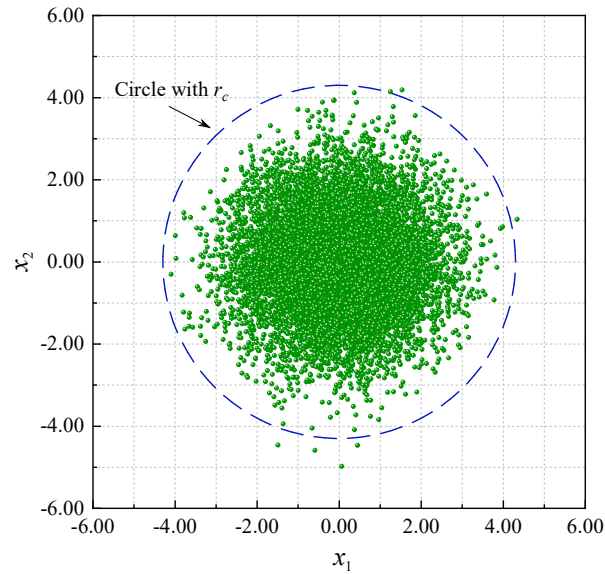


Fig. 3. Distribution of sampling points in standard normal space.

3.2.2. Implementation steps of PSO-AK-MCS

PSO-AK-MCS is a two-level iterative process. The outer iteration involves gradually increasing the data of DoE and improving the Kriging surrogate model. The inner iteration involves implementing PSO. The maximum iteration number serves as the stopping condition for the inner iteration, while $\min(U(\mathbf{x})) \geq 2.0$ is the stopping condition for the outer iteration is detailed in Sec 2.2. It is important to note that during the initial stage of constructing the surrogate model, it is

possible for model updating to stop if the selected ‘high-value sample points’ meet the condition of $\min(U(\mathbf{x})) \geq 2.0$, and finally the ideal surrogate model cannot be obtained. This can occur because there may be significant differences between the performance function obtained from the Kriging model based on the initial data of DoE and the real performance function, resulting in false high-value samples. To address this issue, it is required that the set of DoE \mathbf{S}_{DoE} contain at least one sample point in the vicinity of the limit state surface in this work. The condition for meeting this requirement is expressed as

$$G(\mathbf{x}) < 0.1 \cdot \|\nabla \hat{G}(\mathbf{x})\| \quad (18)$$

where $\nabla \hat{G}(\mathbf{x})$ represents the gradient vector of the predicted performance function value to the random variables, which can be obtained by using the Kriging model.

The main steps of PSO-AK-MCS for reliability analysis are listed as follows:

Step 1: Set control parameters for PSO, including N_{swarm} , $N_{\text{ite_max}}$, ω , c_1 , c_2 and V_{max} .

Step 2: Build the initial data of DoE. Generate the initial set of DoE $\mathbf{S}_{\text{DoE}} = (\mathbf{x}^1, \mathbf{x}^2, \dots, \mathbf{x}^m)$ using Latin Hypercube Sampling (LHS) according to the distribution parameters of random variables, and obtain the performance function values of them denoted as $\mathbf{Y}_{\text{DoE}} = (G(\mathbf{x}^1), G(\mathbf{x}^2), \dots, G(\mathbf{x}^m))$ with m being the number of samples in DoE.

Step 3: Construct the Kriging model according to the data in \mathbf{S}_{DoE} and \mathbf{Y}_{DoE} .

Step 4: Based on the current Kriging model, select a high-value sample through PSO, which includes the following sub-steps:

Step 4-(1): Initialization of particle swarm. Generate particle swarm by randomly initializing the position and velocity of each particle in the solution space. Evaluate all particles in the swarm using Eqs. (16) and set the current position as the historical best position for each particle. Meanwhile, determine the swarm’s best position according to Eq. (15).

Step 4-(2): Update the position and velocity for all particles using Eqs. (12) and (13) and obtain a new generation of particle swarm.

Step 4-(3): Evaluate all particles in the swarm using Eqs. (16), and update the historical best position for each particle and the best position of the whole swarm using Eqs. (14) and (15). If the iteration number does not reach $N_{\text{ite_max}}$, turn to Step 4-(2); otherwise, go to the next step.

Step 4-(4): If the iteration number reaches N_{ite_max} , output the best position of the swarm as the selected high-value sample point.

Step 5: Receive the high-value sampling point $\mathbf{x}^* = \mathbf{X}_{gbest}^{(N_{ite_max})}$ selected by PSO, and check the condition for stopping update of Kriging model. If $U(\mathbf{x}^*) \geq 2.0$, go to **Step 6**; otherwise, obtain the value of performance function $G(\mathbf{x}^*)$ and add \mathbf{x}^* and $G(\mathbf{x}^*)$ to \mathbf{S}_{DoE} and \mathbf{Y}_{DoE} , respectively, then turn to **Step 3**.

Step 6: Generate Monte Carlo population $\mathbf{S}_{MC} = (\mathbf{x}^1, \mathbf{x}^2, \dots, \mathbf{x}^{n_{MC}})$ by Monte Carlo sampling according to the random variables in the system with given distribution parameters.

Step 7: Predict the mean values of performance function $u_{\hat{G}}(\mathbf{x}^i) (i=1, 2, \dots, n_{MC})$ for all samples in the Monte Carlo population $\mathbf{S}_{MC} = (\mathbf{x}^1, \mathbf{x}^2, \dots, \mathbf{x}^{n_{MC}})$ using the established Kriging surrogate model. Then, the estimated failure probability \hat{P}_f can be calculated using Eq. (9).

Step 8: Check the sufficiency of Monte Carlo population through the variation coefficient of failure probability $V_{\hat{P}_f}$ obtained using Eq. (11). If $V_{\hat{P}_f} < 0.05$, output \hat{P}_f and end the program. If $V_{\hat{P}_f} \geq 0.05$, generate a new batch of samples by Monte Carlo sampling according to the distribution characteristics of random variables, add these samples to Monte Carlo population \mathbf{S}_{MC} , and then turn to **Step 7**.

Fig. 4 displays the flow chart of PSO-AK-MCS. It can be observed that PSO-AK-MCS does not require the construction of a CSP. Additionally, there is no need for repeated calculation of the variation coefficient of failure probability during surrogate model construction. This method clearly separates surrogate model construction and failure probability calculation into two distinct stages, resulting in a more transparent implementation process. It is important to emphasize that the proposed method selects high-value samples based on an optimization algorithm rather than a CSP-based method. This addresses the issue of being unable to obtain high-value sample points in sparse distribution regions of candidate samples. With the method proposed in this paper, a Kriging surrogate model for reliability analysis with small failure probability can be constructed without introducing more complex sampling techniques such as importance sampling [32] or subset simulation [20]. This provides a more concise and straightforward approach for reliability analysis.

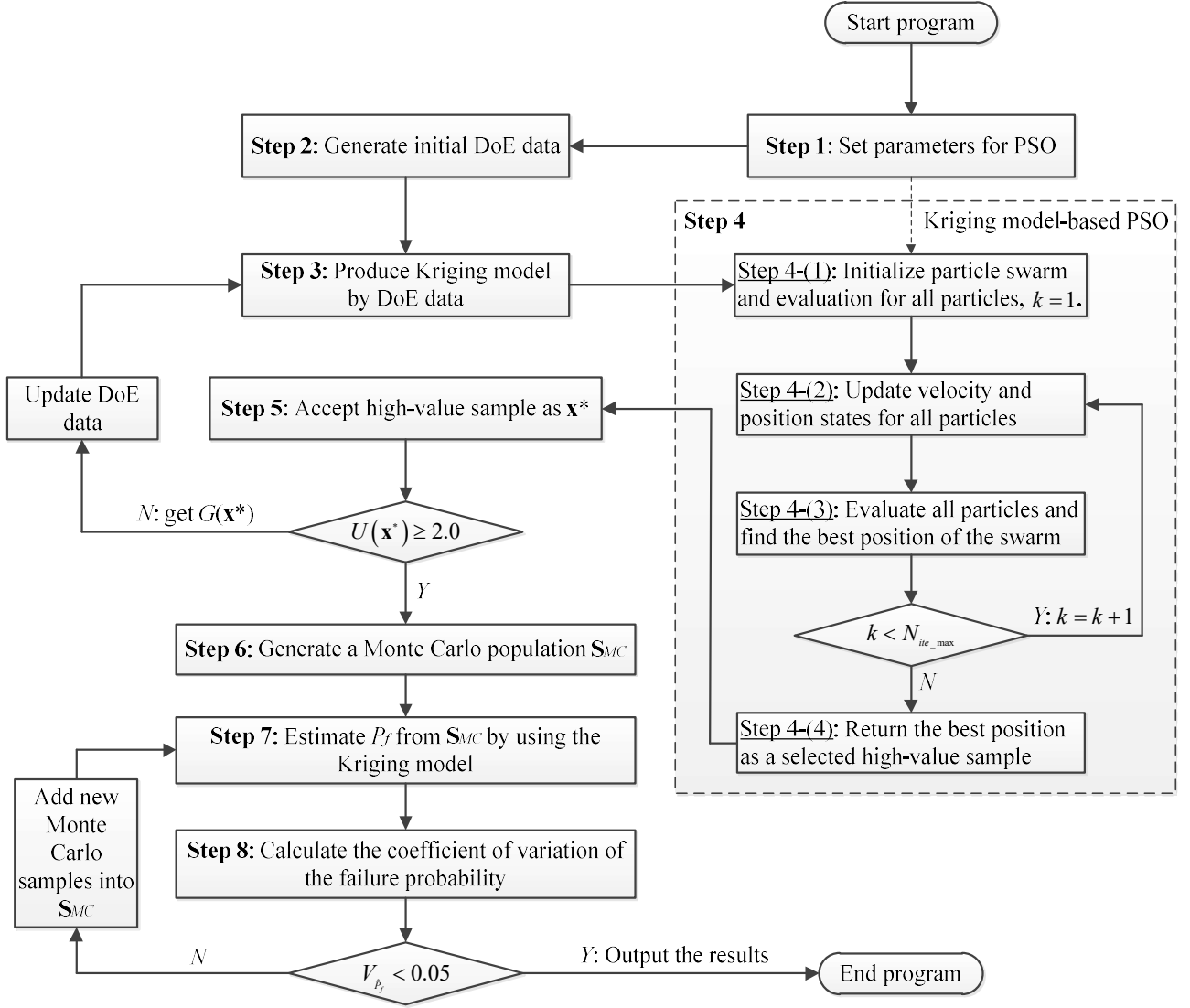


Fig. 4. Flow chart of PSO-AK-MCS.

3.2.3. Modified learning function for PSO-AK-MCS

The optimization capability of PSO allows PSO-AK-MCS to generate new sample points with lower value of $U(\mathbf{x})$ compared to AK-MCS based on CSP. As a result, it is more challenging for the high-value samples generated by PSO-AK-MCS to meet the stopping condition of $\min(U(\mathbf{x})) \geq 2.0$, potentially increasing the final size of the DoE. On the other hand, according to the current definition of the U function, there are points within the given design space with extremely low value of $U(\mathbf{x})$ despite their limited contribution to improving surrogate model accuracy. In PSO-AK-MCS, these points may be discovered through optimization algorithms, increasing the size of the DoE.

The above issue is illustrated using the performance function $G(x) = \sin(x)$, $x \in [\pi/2, 5\pi/2]$.

Assuming that the determined samples of DoE are located at $x=4.0, 6.18, 6.38$, and 7.5 , a Kriging model is constructed based on these samples and the next high-value sample point is located according to the current Kriging model. **Fig. 5** displays the curves of $\mu_{\hat{G}}(x)$, $\mu_{\hat{G}}(x) \pm \sigma_{\hat{G}}(x)$ and $U(x)$ (expressed by $\log_{10} U(x)$) based on the current Kriging model. From the figure, it can be observed that the minimum value of $U(x)$ appears near $x^* = 2\pi$ in the current state. In other words, even though the DoE samples already contain the two points near $x^* = 2\pi$ ($x = 6.18$ and $x = 6.38$), resulting in a very small Kriging variance $\sigma_{\hat{G}}^2(x)$ in this narrow range, the minimum value remains in this range (point A in the figure) due to the existence of $\mu_{\hat{G}}(x) = 0$ between $x = 6.18$ and $x = 6.38$. An effective optimization algorithm can identify point A and add it to DoE. However, the Kriging surrogate model constructed based on the new DoE data still shows an extremely low value of $U(\mathbf{x})$ near point A . In fact, when points at $x = 6.18$ and $x = 6.38$ are included in DoE, point A 's contribution to the Kriging model is quite limited. For the current Kriging model shown in **Fig. 5**, point B is a valuable sample point due to its high Kriging variance and low absolute value of the predicted mean $|\mu_{\hat{G}}(x)|$. Assuming that point B can be selected and added to DoE, the subsequent Kriging model has a minimum value near point C . Thus, a point near point C can be identified as a high-value sample point in the following process. After adding this sample point to DoE, the established Kriging model performs well in distinguishing between failure and safe regions.

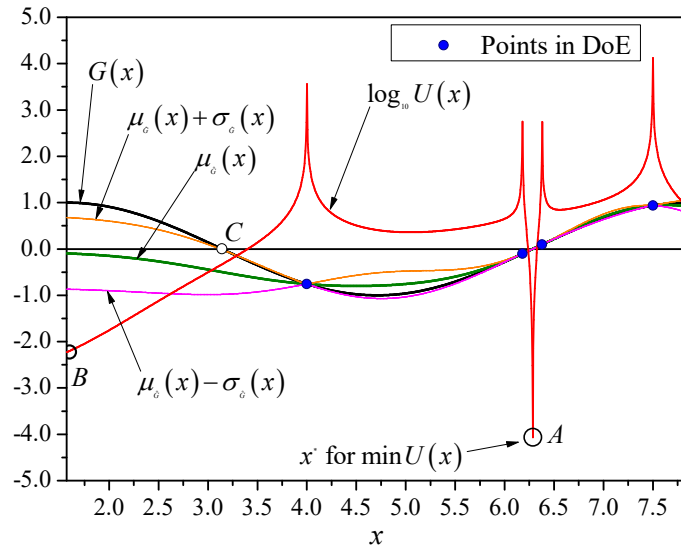


Fig. 5. Graphics for discussion on the learning function U .

Given the reasonably strong optimization capability, the key to addressing the above issue is to

effectively adjust the learning function. This paper proposes the following two schemes of modified learning function.

(1) Modified learning function with local neighborhood effect considered

As depicted in **Fig. 5**, for a point that exhibits a minimum value of $U(x)$ but lacks a high value for constructing a surrogate model, such as point A , rapid changes to the value of $U(x)$ are observed in its vicinity. It is deemed imprudent to evaluate the value of a point while disregarding the influence of its neighborhood. Therefore, a modified learning function $\tilde{U}(\mathbf{X})$ considering local neighborhood effects is defined as follows:

$$\tilde{U}(\mathbf{X}) = \frac{1}{N_{\text{rev}} + 1} \left[U(\mathbf{X}) + \sum_{i=1}^{N_{\text{rev}}} U(\mathbf{X} + \Delta\mathbf{X}^{(i)}) \right] \quad (19)$$

where N_{rev} indicates the number of neighboring points considered for \mathbf{X} , and $\Delta\mathbf{X}^{(i)}$ represents the offset amount relative to the i^{th} neighboring point, which is obtained by

$$\Delta\mathbf{X}^{(i)} = 2.0r_{\text{rev}}(\text{rand} - 0.5, \text{rand} - 0.5) \quad (20)$$

where r_{rev} represents a parameter used to describe the offset range. Accordingly, the definition of the objective function for PSO is rewritten as

$$F_{\text{obj}}(\mathbf{X}) = \tilde{U}(\mathbf{X}) + p \cdot (\|\mathbf{X}\| - r_c) \quad (21)$$

(2) Modified learning function with distribution of DOE samples considered

As shown in **Fig. 5**, point A , which exhibits a minimum value of $U(x)$ but lacks a high value for constructing a surrogate model, is situated in the immediate vicinity of the existing DOE sample points. To circumvent this issue, it is proposed that the next high-value sample should maintain a certain distance from the existing DOE sample points. Consequently, the modified learning function $\hat{U}(\mathbf{X})$ is defined as follows:

$$\hat{U}(\mathbf{X}) = U(\mathbf{X}) + 2.0\delta \quad (22)$$

where

$$\delta = \begin{cases} 0, & \|\mathbf{X} - \mathbf{x}^i\| > r_{\text{rev}} \text{ for all } \mathbf{x}^i \in \text{DoE} \\ 1, & \text{otherwise} \end{cases} \quad (23)$$

where r_{rev} represents a parameter used to describe the offset range. The aforementioned modified learning function can be interpreted as augmenting the learning function value by 2.0 when the distance between the position of point \mathbf{X} and any sample \mathbf{x}^i in the current DOE is less than the specified parameter r_{rev} . Correspondingly, the stop condition for the Kriging model update process

is $\min(\widehat{U}(\mathbf{x})) \geq 2.0$. Accordingly, the definition of the objective function for PSO is reformulated as

$$F_{\text{obj}}(\mathbf{X}) = \widehat{U}(\mathbf{X}) + p \cdot (\|\mathbf{X}\| - r_c) \quad (24)$$

4. Validation

Numerical examples are used to validate the effectiveness of the proposed method. Firstly, a series system with four branches is employed to investigate the effectiveness of the PSO algorithm in identifying high-value samples (Sec. 4.1) and to evaluate the influence of utilizing the modified learning functions on the PSO-AK-MCS method (Sec. 4.2). The performance function of the system is shown in Eq. (25), where x_1 and x_2 are independent standard normal distributed random variables.

$$G(x_1, x_2) = \min \begin{cases} 3.0 + 0.1 \times (x_1 - x_2)^2 - (x_1 + x_2)/\sqrt{2} \\ 3.0 + 0.1 \times (x_1 - x_2)^2 + (x_1 + x_2)/\sqrt{2} \\ (x_1 - x_2) + 6.0/\sqrt{2} \\ (x_2 - x_1) + 6.0/\sqrt{2} \end{cases} \quad (25)$$

Subsequently, a series system with two branches is used to show the superiority of the proposed method in small failure probability problems (Sec. 4.3). The performance function of this system is shown in Eq. (26), where x_1 and x_2 are independent standard normal distributed random variables, and k is a parameter to adjust the failure probability.

$$G(x_1, x_2) = \min \begin{cases} k + 0.1 \times (x_1 - x_2)^2 - (x_1 + x_2)/\sqrt{2} \\ k + 0.1 \times (x_1 - x_2)^2 + (x_1 + x_2)/\sqrt{2} \end{cases} \quad (26)$$

4.1. Effectiveness of PSO

The failure probability of the system is evaluated using both the crude Monte Carlo Simulation (MCS) method and the PSO-AK-MCS method. In MCS, random sampling is conducted according to the standard normal distribution and the Monte Carlo population is set to 1×10^6 . In PSO-AK-MCS, the control parameters for PSO are set to $N_{\text{swarm}} = 50$, $N_{\text{ite_max}} = 50$, $V_{\text{max}} = 0.3$, $\omega = 0.729$ and $c_1 = c_2 = 2.0$. Generally, the optimization ability of PSO increases with the increase of N_{swarm} and $N_{\text{ite_max}}$. Based on the authors' previous experience, these settings ensure that PSO has sufficient optimization ability. The sign indication learning function $U(\mathbf{X})$ is used in the objective function and the number of samples for the initial DoE is set to 6. In the second stage to determine the failure probability, the scale of Monte Carlo population \mathbf{S}_{MC} is initially set to

size(\mathbf{S}_{MC}) = 5×10^4 . If it is determined that the Monte Carlo population is insufficient when checking its sufficiency of $V_{\hat{P}_f} \geq 0.05$, an additional 5×10^4 samples are generated and add to \mathbf{S}_{MC} .

Table 1 presents the results obtained using MCS and PSO-AK-MCS, where P_f refers to the failure probability, N_G represents number of calling the real performance function, ε_{P_f} represents the relative error of failure probability between surrogate model methods and MCS, calculated as

$$\varepsilon_{P_f} = \frac{|P_{f,\text{surrogate}} - P_{f,\text{MCS}}|}{P_{f,\text{MCS}}} \times 100\% \quad (27)$$

where $P_{f,\text{MCS}}$ is the failure probability obtained by MCS and $P_{f,\text{surrogate}}$ represents the failure probability obtained by a surrogate model method. As shown by **Table 1**, PSO-AK-MCS achieves satisfactory accuracy. The numbers of times the real performance function is called by PSO-AK-MCS is 171, and the relative error of the failure probability is 0.057%.

Table 1 Failure probability of the series system with four branches.

Method	$P_f / 10^{-2}$	$\varepsilon_{P_f} / \%$	N_G
MCS	0.4341	-	1×10^6
PSO-AK-MCS	0.4339	0.057	171

Fig. 6 illustrates the changes in the limit state curves for PSO-AK-MCS, including the limit state curves when the number of samples in DoE is 21, 36, and 51, as well as the final state of the surrogate model. In these figures, the red dotted line represents the real limit state curves corresponding to the real performance function, while the blue line represents the limit state curves predicted by the surrogate model. The star points represent the initial sample points generated by LHS and the round white points represent the sample points added during the process of updating surrogate model. As shown in the figures, as DoE increases, the limit state curves of the surrogate model become increasingly closer to the real limit state curves. The final predicted limit state curves can accurately distinguish between failure and safe points, as shown in **Fig. 7**.

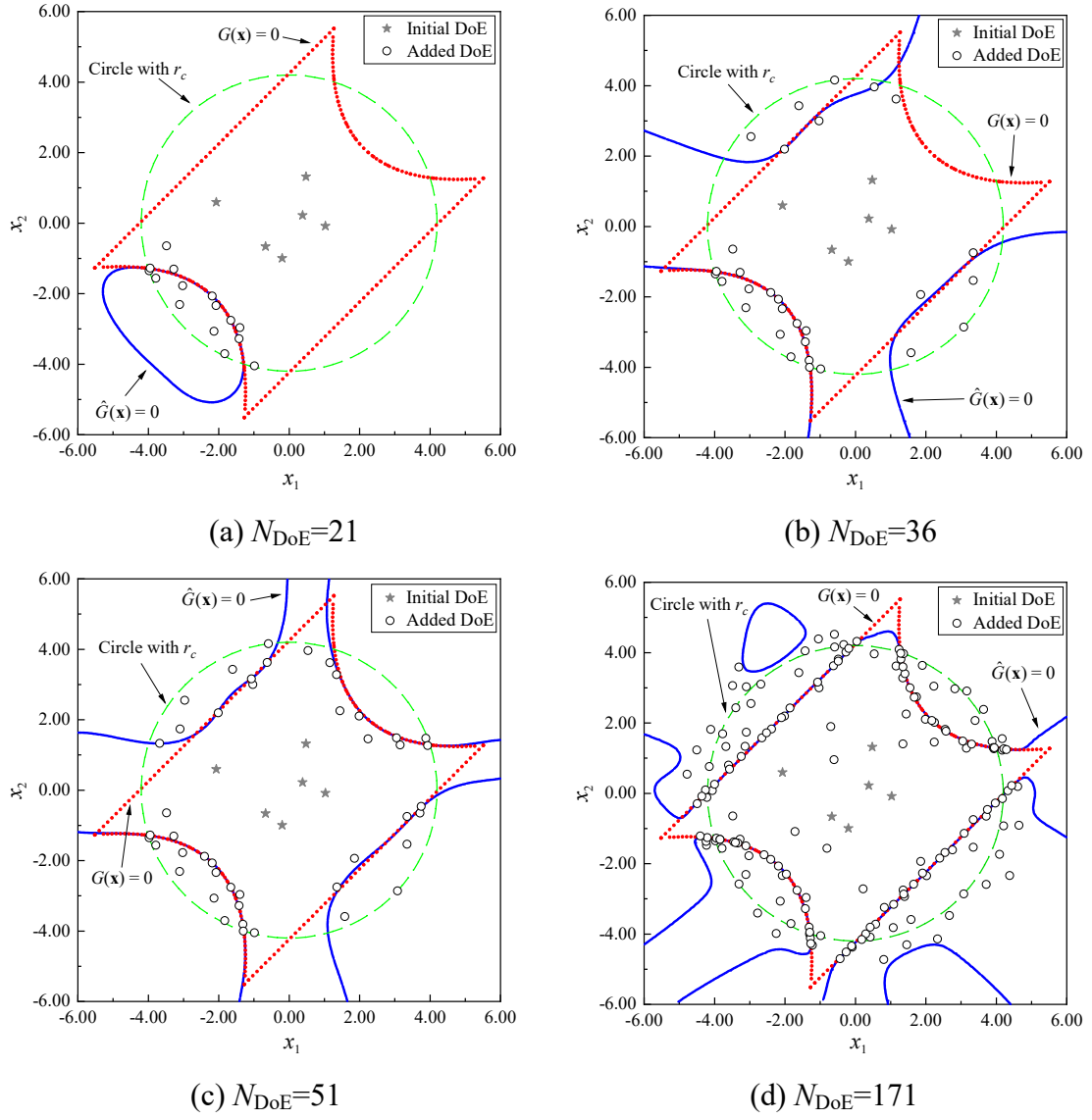


Fig. 6. The predicted limit states of PSO-AK-MCS in evolution process.

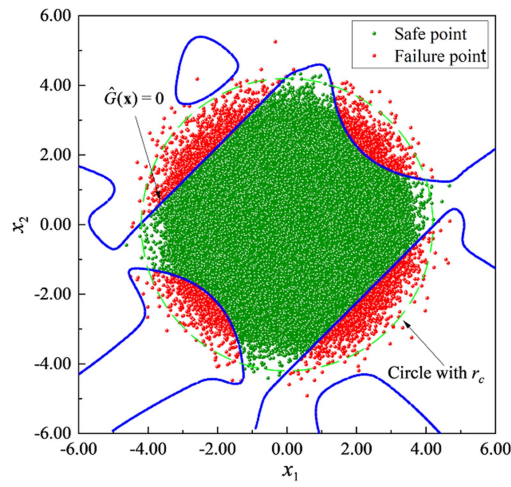


Fig. 7. Predicted limit state curves and distribution of safe and failure points.

Unlike AK-MCS with CSP, PSO-AK-MCS obtains high-value samples through intelligent search based on PSO. **Fig. 8** illustrates the relationship between the sample points in DoE and the objective function value during the process of updating the surrogate model in PSO-AK-MCS. It specifically describes the distribution of the objective function value when the scale of DoE is 21, 36, 51, and 171. As shown in **Fig. 8**, the high-value sample points (green points) found using PSO are located in positions where the objective function value is smaller (dark blue region) under the prediction of the current surrogate model. This verifies the effectiveness of PSO's optimization process. Furthermore, the selection of a single high-value sample point using PSO is investigated. **Fig. 9** shows the process of obtaining the 21th sample point for DoE, including the distribution of initially generated particles and their distribution after 15, 30, and 50 iterations. The red arrows in **Fig. 9** depict the motion direction of particles in the next iteration. As iterations progress, particles move closer together and eventually obtain the best position of the swarm in a region with a relatively dense distribution of particles. This again indicates that calling PSO in the proposed adaptive surrogate model method is effective. During PSO, some particles remain far from the best position of the swarm, reflecting the algorithm's ability to escape local optima.

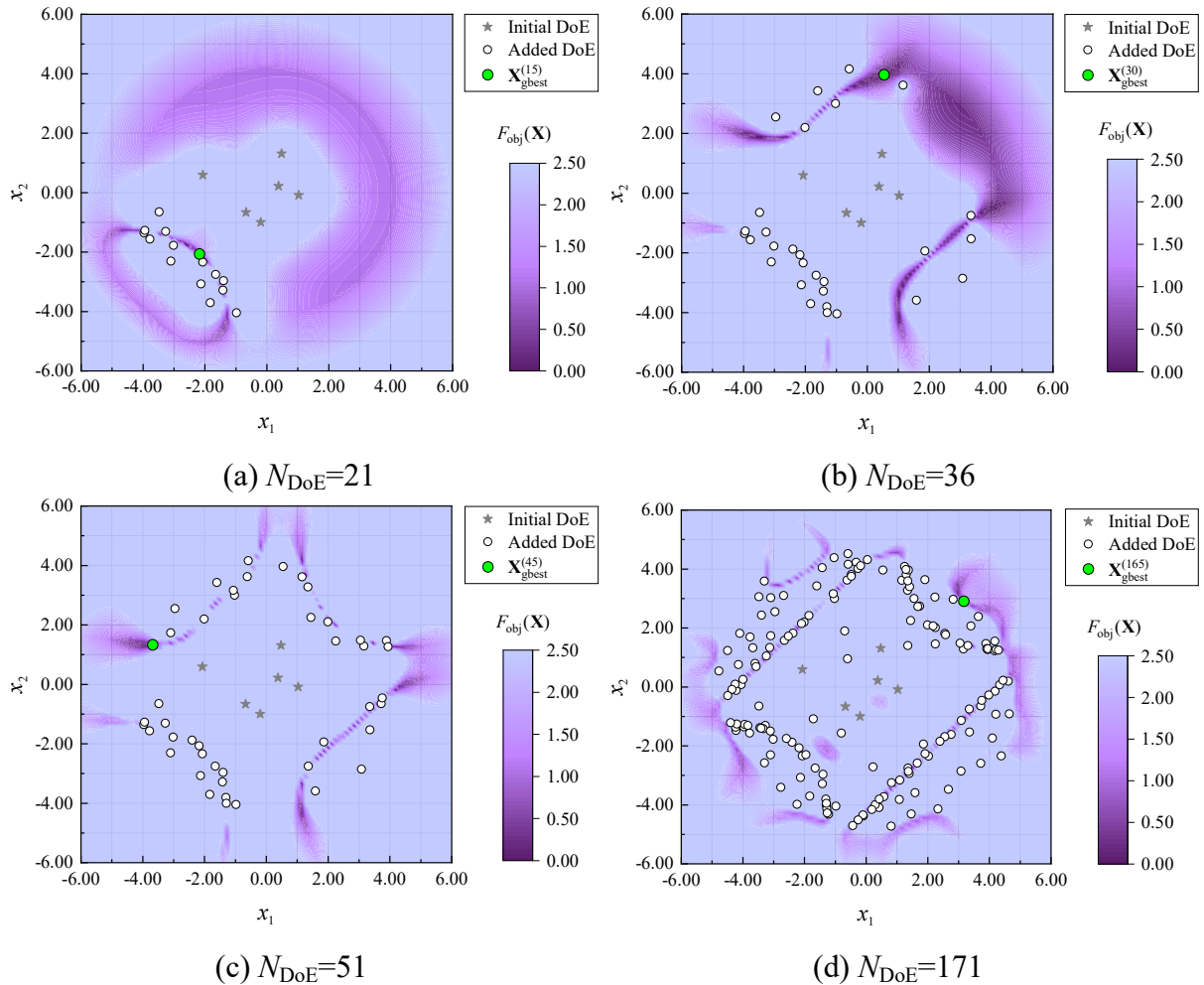


Fig. 8. Distribution of objective function and high-value sample points.

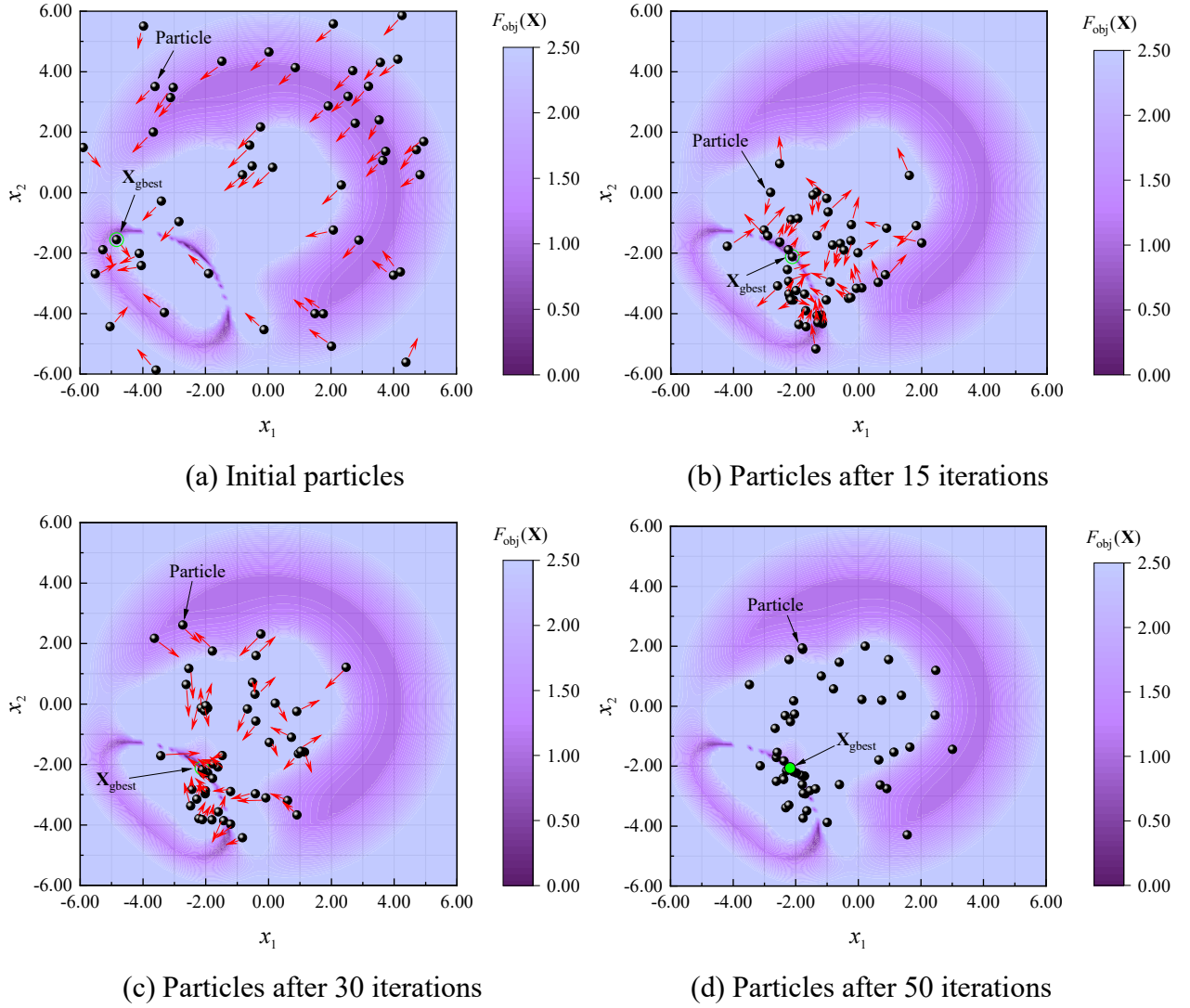


Fig. 9. Demonstration of PSO optimization process for $N_{\text{DoE}}=21$.

4.2. Impact of modified learning function

For the series system with four branches (Eq. (25)), PSO-AK-MCS with the modified learning functions $\tilde{U}(\mathbf{X})$ and $\hat{U}(\mathbf{X})$ is used to calculate the failure probability. For the modified learning function $\tilde{U}(\mathbf{X})$, the parameter indicating the number of neighboring points is set to $N_{\text{rev}} = 4$ and the parameter describing the offset range is set to $r_{\text{rev}} = 0.01, 0.02, 0.04$, respectively. For the modified learning function $\hat{U}(\mathbf{X})$, the parameter describing the offset range is set to $r_{\text{rev}} = 0.1, 0.2, 0.3, 0.4$, respectively. **Table 2** lists the statistical results of 20 calculations and results from some references. The average failure probability of MCS is used to calculate the relative errors of failure probabilities for various methods. In **Table 2**, \bar{N}_{DoE} represents the average number of

samples in DoE used to construct the surrogate models, $\bar{\varepsilon}_{P_f}$ refers to the relative error of failure

probability between the surrogate model methods and MCS. For MCS, $\bar{P}_f = \bar{P}_{f,\text{MCS}} = \frac{1}{20} \sum_{i=1}^{20} P_{f,\text{MCS}}^{(i)}$

is the average value of failure probabilities obtained by 20 calculations, denoted as

$P_{f,\text{MCS}}^{(i)} (i=1,2,\dots,20)$. For PSO-AK-MCS, $\bar{\varepsilon}_{P_f}$ is obtained by

$$\bar{\varepsilon}_{P_f} = \frac{1}{20} \sum_{i=1}^{20} \varepsilon_{P_f}^{(i)} \quad (28)$$

where $\varepsilon_{P_f}^{(i)} (i=1,2,\dots,20)$ is the relative error of failure probability for the i^{th} calculation, expressed as

$$\varepsilon_{P_f}^{(i)} = \frac{|P_{f,\text{surrogate}}^{(i)} - P_{f,\text{MCS}}^{(i)}|}{P_{f,\text{MCS}}^{(i)}} \times 100\% \quad (29)$$

and \bar{P}_f is the average value of failure probabilities obtained by $\bar{P}_f = (1 - \bar{\varepsilon}_{P_f}) \bar{P}_{f,\text{MCS}}$.

Table 2 Summary of the results for the series system with four branches.

Method	r_{rev}	$\bar{P}_f / 10^{-2}$	$\bar{\varepsilon}_{P_f} / \%$	\bar{N}_{DoE}
MCS	-	0.4455	-	1×10^6
PSO-AK-MCS with $U(\mathbf{X})$	-	0.4454	0.059	182.4
PSO-AK-MCS with $\tilde{U}(\mathbf{X})$	0.01	0.4440	0.337	138.6
	0.02	0.4435	0.446	110.9
	0.04	0.4431	0.636	105.2
PSO-AK-MCS with $\hat{U}(\mathbf{X})$	0.10	0.4452	0.064	167.3
	0.20	0.4447	0.182	133.0
	0.30	0.4439	0.367	108.8
	0.40	0.4416	0.884	89.4
AK-MCS-U [30]	-	0.4416	0.880	126
AK-MCS-EFF [30]	-	0.4412	0.970	124
Directional Sampling (DS) [27]	-	0.45	1.010	52
DS+Spline [27]	-	0.24	46.128	145
DS+Nerual Network [27]	-	0.41	7.968	165

As shown by **Table 2**, PSO-AK-MCS with $U(\mathbf{X})$ has extremely high accuracy but a

relatively large DOE size. For PSO-AK-MCS with $\tilde{U}(\mathbf{X})$ or $\hat{U}(\mathbf{X})$, as the parameter r_{rev} increases, there is a progressive reduction in the size of DoE required to construct the surrogate model in PSO-AK-MCS, while the relative error of failure probability increases at a slow rate. This means that by changing the parameter r_{rev} , the learning function that takes into account local neighborhood effects can be used to adjust the accuracy and efficiency of the solution. By using $\tilde{U}(\mathbf{X})$ with $r_{\text{rev}} = 0.02$ or $\hat{U}(\mathbf{X})$ with $r_{\text{rev}} = 0.30$, the relative error of the failure probability remains within 0.5% and the size of DoE approaches about 110, providing a fine balance between accuracy and computational efficiency.

4.3. Performance in small failure probability problems

A series system with two branches is considered, with its performance function shown in Eq. (26). This study evaluates the cases of $k = 3.4$ and $k = 3.9$. The failure probability of the system is obtained using the crude Monte Carlo Simulation (MCS) method, AK-MCS [30], and the proposed PSO-AK-MCS.

In MCS, the Monte Carlo populations are set to 1×10^6 and 8×10^6 for the cases of $k = 3.4$ and $k = 3.9$, respectively. In AK-MCS, the number of samples in the initial DoE is set to 6. The scale of Monte Carlo population \mathbf{S}_{MC} at the start is set to $\text{size}(\mathbf{S}_{MC}) = 5 \times 10^4$. If $V_{\hat{P}_f} \geq 0.05$ when checking the sufficiency of the Monte Carlo population, an additional 5×10^4 samples are generated and add to \mathbf{S}_{MC} . The failure probabilities for the two cases are obtained by evaluating the 1×10^6 and 8×10^6 samples in MCS using the established Kriging surrogate model. In PSO-AK-MCS, the control parameters for PSO are set to $N_{\text{swarm}} = 100$, $N_{\text{ite_max}} = 50$, $V_{\text{max}} = 0.3$, $\omega = 0.729$ and $c_1 = c_2 = 2.0$. Especially, the modified learning function with $N_{\text{rev}} = 4$ are used to select the high-value samples, respectively. Similar to AK-MCS, 1×10^6 and 8×10^6 samples in MCS are evaluated using the established surrogate model to calculate the failure probabilities for the two cases, respectively. To ensure the reliability of the results, 20 calculations are carried out for each case.

For the two cases, the statistical results of 20 calculations are summarized in **Table 3** and **Table 4**, where \bar{N}_{EST} represents the average number of times for predicting the performance function value during the process of constructing the surrogate models, \bar{T} is the average computational time and $\bar{\varepsilon}_{P_f}$ refers to the average relative error of failure probability between the surrogate model methods and MCS. In **Table 3** and **Table 4**, \bar{P}_f is the representative value of

failure probability. For MCS, \bar{P}_f is the average value of failure probabilities obtained by 20 calculations, while for other methods, $\bar{P}_f = (1 - \bar{\varepsilon}_{P_f}) \bar{P}_{f,\text{MCS}}$.

Table 3 Results for the case of $k = 3.4$.

Method	r_{rev}	$\bar{P}_f / 10^{-4}$	$\bar{\varepsilon}_{P_f} / \%$	\bar{N}_{DoE}	\bar{T} / s	\bar{N}_{EST}
MCS	-	4.2495	-	-	-	-
AK-MCS	-	4.2405	0.211	38.55	86.73	1.460×10^7
PSO-AK-MCS with $U(\mathbf{X})$	-	4.2449	0.109	47.85	2.98	1.949×10^5
PSO-AK-MCS with $\tilde{U}(\mathbf{X})$	0.01	4.2421	0.174	42.33	4.65	8.654×10^5
	0.02	4.2406	0.210	40.40	4.28	8.403×10^5
PSO-AK-MCS with $\hat{U}(\mathbf{X})$	0.10	4.2434	0.143	41.40	3.34	1.684×10^5
	0.20	4.2409	0.202	39.90	3.21	1.622×10^5
	0.30	4.2373	0.286	37.75	3.05	1.524×10^5
	0.40	4.2340	0.365	35.25	2.85	1.435×10^5

Table 4 Results for the case of $k = 3.9$.

Method	r_{rev}	$\bar{P}_f / 10^{-5}$	$\bar{\varepsilon}_{P_f} / \%$	\bar{N}_{DoE}	\bar{T} / s	\bar{N}_{EST}
MCS	-	5.8337	-	-	-	-
AK-MCS	-	5.8205	0.226	42.03	6785.64	5.004×10^8
PSO-AK-MCS with $U(\mathbf{X})$	-	5.8263	0.127	39.41	16.82	1.750×10^5
PSO-AK-MCS with $\tilde{U}(\mathbf{X})$	0.01	5.8256	0.138	37.49	26.46	8.234×10^5
	0.02	5.8229	0.185	36.05	26.07	8.004×10^5
PSO-AK-MCS with $\hat{U}(\mathbf{X})$	0.10	5.8256	0.139	38.95	17.03	1.723×10^5
	0.20	5.8249	0.150	37.05	16.84	1.653×10^5
	0.30	5.8231	0.181	35.10	15.40	1.524×10^5
	0.40	5.8122	0.368	33.60	14.73	1.430×10^5

Under the setting of $k = 3.4$, the system's failure probability is about 4.25×10^{-4} . As shown in **Table 3**, both AK-MCS and PSO-AK-MCS achieve high accuracy, with the average errors in failure probabilities within 0.3%. The number of DoE samples required to construct the surrogate model in PSO-AK-MCS with $U(\mathbf{X})$ is greater than that of AK-MCS. This can be attributed to the optimization algorithm's ability to find points with lower objective function value in the design space, thus delaying the surrogate model's construction process. In terms of computational time,

PSO-AK-MCS takes significantly less time than AK-MCS due to the difference in the number of performance function value predictions. In each calculation, AK-MCS predicts approximately 1.460×10^7 performance function values while PSO-AK-MCS with $U(\mathbf{X})$ predicts only about 1.95×10^5 , resulting in significantly less time consumption for PSO-AK-MCS. By using the modified learning functions, such as $\tilde{U}(\mathbf{X})$ with $r_{\text{rev}} = 0.02$ and $\hat{U}(\mathbf{X})$ with $r_{\text{rev}} = 0.20$, the number of DoE samples required for constructing the surrogate model can be further reduced while maintaining an acceptable relative error in failure probability.

Under the setting of $k = 3.9$, the failure probability is reduced by an order of magnitude than that under the setting of $k = 3.4$, and the difficulty of reliability analysis is significantly increased. As shown by **Table 4**, the number of DoE samples required for PSO-AK-MCS to construct the surrogate model is less than that of AK-MCS. To ensure the reliability of the estimated failure probability, AK-MCS requires a large number of candidate samples, resulting in a sharp increase in the number of performance function value predictions during surrogate model construction and a corresponding increase in computational time. As indicated in **Table 4**, AK-MCS predicts approximately 5.004×10^8 performance function values for candidate samples during surrogate model construction, resulting in a computational time of nearly 2 hours. In contrast, PSO-AK-MCS with $U(\mathbf{X})$ predicts only 1.750×10^5 performance function values during surrogate model construction, resulting in a computational time that is only 1/400 of that of AK-MCS. Due to its ability to more accurately locate high-value sample points through optimization algorithms, PSO-AK-MCS achieves extremely high surrogate model accuracy with an average error in failure probability of only 0.127%. By using the modified learning functions, such as $\tilde{U}(\mathbf{X})$ with $r_{\text{rev}} = 0.02$ and $\hat{U}(\mathbf{X})$ with $r_{\text{rev}} = 0.30$, the scale of DOE can be further reduced while maintaining an acceptable relative error in failure probability, playing an important role in improving the efficiency of reliability analysis in practical engineering. Compared with PSO-AK-MCS with $\tilde{U}(\mathbf{X})$ where more performance function value predictions are required to evaluate the performance function value predictions, PSO-AK-MCS with $\hat{U}(\mathbf{X})$ demonstrates higher solution efficiency.

Fig. 10 illustrates the distribution of failure points, the real limit state curves, and the predicted limit state curves obtained by PSO-AK-MCS and their evolution. The numbers of DoE samples required to construct the final surrogate models under the settings of $k = 3.4$ and $k = 3.9$ are 48 and 42, respectively. The figure depicts the predicted limit state curves of surrogate models with 10,

20, and 30 DoE samples, respectively, as well as those of the final surrogate models. The predicted limit state curves under various N_{DoE} conditions are represented by solid lines of different colors, while the actual limit state curves are represented by black dotted lines. It can be observed that as the number of DoE samples increases, the predicted limit state curves of the surrogate model gradually converge towards the actual limit state curves. Ultimately, failure points can be accurately incorporated into the predicted failure regions to obtain an accurate failure probability.

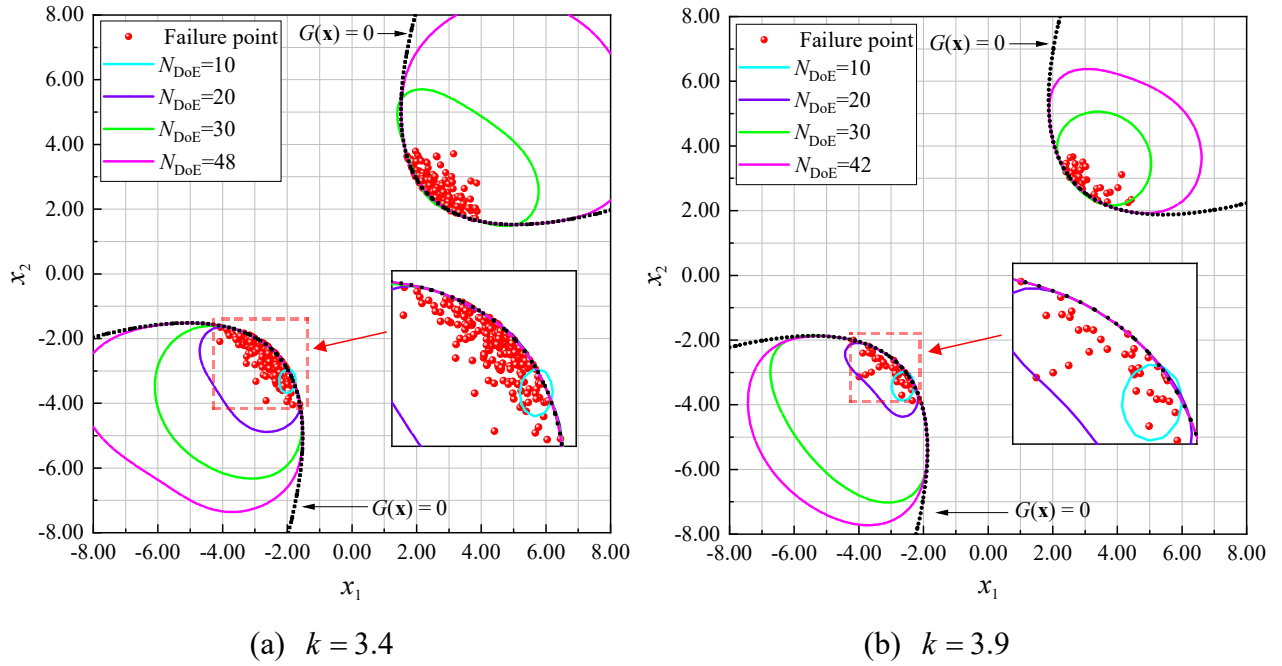


Fig. 10. Distribution of failure points and the predicted limit states.

5. Conclusions

This study proposes a novel adaptive Kriging surrogate model method combined with a particle swarm optimization algorithm for reliability analysis with small failure probabilities. During implementation, the surrogate model is iteratively improved and high-value samples are selected for updating the surrogate model through an optimization solution using the particle swarm optimization algorithm. In addition, two modified learning functions considering local neighborhood effects and distribution distance of DoE samples, respectively, are proposed. Numerical examples are used to validate the proposed method and evaluate its computational performance. The following conclusions can be drawn:

(1) The incorporation of a particle swarm optimization algorithm effectively increases the likelihood of obtaining high-value samples for constructing the surrogate model, resulting in an improvement in solution accuracy for an adaptive Kriging surrogate model method in reliability

analysis. Results demonstrate that the proposed method achieves satisfactory computational performance by fully leveraging the global optimization capabilities of the PSO algorithm.

(2) Combining adaptive surrogate model methods with a particle swarm optimization algorithm can address the poor computational performance caused by the distribution defect of candidate samples in CSP-based adaptive surrogate model methods. Results indicate that the proposed method is advantageous in handling small failure probabilities in reliability analysis.

(3) The modified learning functions, which take neighborhood influence and distribution distance of DoE samples into account, respectively, can be used to more reasonably select high-value samples for updating the surrogate model, thereby improving the performance of the adaptive surrogate model method. Results illustrate that the proposed surrogate model method with modified learning function is advantageous in terms of both solution accuracy and computational efficiency.

Despite the utilization of only rudimentary numerical examples, they suffice in corroborating the efficacy of the proposed methodology. For problems involving random variables with different distribution characteristics, Monte Carlo sampling can still be executed in accordance with the standard normal distribution, necessitating a specific transformation to account for the influence of the actual distribution prior to computing the performance function. For the reliability assessment of actual engineering structures exhibiting multiple failure modes, the failure probability can be ascertained through Monte Carlo sampling with the adaptive surrogate model, provided that the impact of disparate failure modes is suitably incorporated into the performance function. Consequently, the proposed adaptive surrogate model methodology can be readily extrapolated to address challenges such as various types of random variables and multiple failure modes, thereby offering robust solutions for real-world applications.

Acknowledgments

The project is funded by the National Natural Science Foundation of China (Grant No. 52178209, Grant No. 51878299) and Guangdong Basic and Applied Basic Research Foundation, China (Grant No. 2020A1515010611, Grant No. 2021A1515012280).

References

- [1] Wang C, Matthies HG. Epistemic uncertainty-based reliability analysis for engineering system with hybrid evidence and fuzzy variables. *Computer Methods in Applied Mechanics and Engineering* 2019;

355: 438-55.

- [2] Lee JY, Ellingwood BR. A decision model for intergenerational life-cycle risk assessment of civil infrastructure exposed to hurricanes under climate change. *Reliability Engineering & System Safety* 2017; 159: 100-07.
- [3] Liu HB, Jiang C, Jia XY, Long XY, et al. A new uncertainty propagation method for problems with parameterized probability-boxes. *Reliability Engineering & System Safety* 2018; 172: 64-73.
- [4] Wu J, Zhang D, Liu J, Han X. A moment approach to positioning accuracy reliability analysis for industrial robots. *IEEE Transactions On Reliability* 2020; 69: 699-714.
- [5] Lemaire M. *Structural Reliability*. Hoboken: John Wiley & Sons, 2009.
- [6] Huang X, Li Y, Zhang Y, Zhang X. A new direct second-order reliability analysis method. *Applied Mathematical Modelling* 2018; 55: 68-80.
- [7] Yang M, Zhang D, Cheng C, Han X. Reliability-based design optimization for RV reducer with experimental constraint. *Structural and Multidisciplinary Optimization* 2021; 63: 2047-64.
- [8] Au SK, Beck JL. A new adaptive importance sampling scheme for reliability calculations. *Structural Safety* 1999; 21: 135-58.
- [9] Gao K, Gao W, Wu B, Song C. Nondeterministic dynamic stability assessment of Euler-Bernoulli beams using Chebyshev surrogate model. *Applied Mathematical Modelling* 2019; 66: 1-25.
- [10] Wang Q, Li Q, Wu D, Yu Y, et al. Machine learning aided static structural reliability analysis for functionally graded frame structures. *Applied Mathematical Modelling* 2020; 78: 792-815.
- [11] Rajashekhar MR, Ellingwood BR. A new look at the response surface approach for reliability analysis. *Structural Safety* 1993; 12: 205-20.
- [12] Zhao W, Fan F, Wang W. Non-linear partial least squares response surface method for structural reliability analysis. *Reliability Engineering & System Safety* 2017; 161: 69-77.
- [13] Tan X, Bi W, Hou X, Wang W. Reliability analysis using radial basis function networks and support vector machines. *Computers and Geotechnics* 2011; 38: 178-86.
- [14] Dubourg V, Sudret B, Bourinet J. Reliability-based design optimization using kriging surrogates and subset simulation. *Structural and Multidisciplinary Optimization* 2011; 44: 673-90.
- [15] Chojaczyk AA, Teixeira AP, Neves LC, Cardoso JB, et al. Review and application of Artificial Neural

Networks models in reliability analysis of steel structures. *Structural Safety* 2015; 52: 78-89.

- [16] Yun Y, Min Y, Nakayama H. Multi-objective optimization based on meta-modeling by using support vector regression. *Optimization & Engineering* 2009; 10: 167-81.
- [17] Feng J, Liu L, Wu D, Li G, et al. Dynamic reliability analysis using the extended support vector regression (X-SVR). *Mechanical Systems and Signal Processing* 2019; 126: 368-91.
- [18] Queipo NV, Nava E. A gradient boosting approach with diversity promoting measures for the ensemble of surrogates in engineering. *Structural and Multidisciplinary Optimization* 2019; 60: 1289-311.
- [19] Chen L, Qiu H, Jiang C, Cai X, et al. Ensemble of surrogates with hybrid method using global and local measures for engineering design. *Structural and Multidisciplinary Optimization* 2018; 57: 1711-29.
- [20] Bourinet JM, Deheeger F, Lemaire M. Assessing small failure probabilities by combined subset simulation and Support Vector Machines. *Structural Safety* 2011; 33: 343-53.
- [21] Pan Q, Dias D. An efficient reliability method combining adaptive Support Vector Machine and Monte Carlo Simulation. *Structural Safety* 2017; 67: 85-95.
- [22] Zhang T, Zeng P, Li T, Sun X. System reliability analysis of slopes based on active-learning radial basis function. *Rock and Soil Mechanics*. 2020; 41: 3098-108 (in Chinese).
- [23] Li X, Gong C, Gu L, Gao W, et al. A sequential surrogate method for reliability analysis based on radial basis function. *Structural Safety* 2018; 73: 42-53.
- [24] Xiao N, Zuo MJ, Zhou C. A new adaptive sequential sampling method to construct surrogate models for efficient reliability analysis. *Reliability Engineering & System Safety* 2018; 169: 330-38.
- [25] Sundar VS, Shields MD. Surrogate-enhanced stochastic search algorithms to identify implicitly defined functions for reliability analysis. *Structural Safety* 2016; 62: 1-11.
- [26] Papadopoulos V, Giovanis DG, Lagaros ND, Papadrakakis M. Accelerated subset simulation with neural networks for reliability analysis. *Computer Methods in Applied Mechanics and Engineering* 2012; 223-224: 70-80.
- [27] Schueremans L, Van Gemert D. Benefit of splines and neural networks in simulation based structural reliability analysis. *Structural Safety* 2005; 27: 246-61.

- [28] Ma Y, Liu M, Nan H, Li H, et al. A novel hybrid adaptive scheme for Kriging-based reliability estimation – A comparative study. *Applied Mathematical Modelling* 2022; 108: 1-26.
- [29] Xiao N, Zuo MJ, Guo W. Efficient reliability analysis based on adaptive sequential sampling design and cross-validation. *Applied Mathematical Modelling* 2018; 58: 404-20.
- [30] Echard B, Gayton N, Lemaire M. AK-MCS: An active learning reliability method combining Kriging and Monte Carlo Simulation. *Structural Safety* 2011; 33: 145-54.
- [31] Fauriat W, Gayton N. AK-SYS: An adaptation of the AK-MCS method for system reliability. *Reliability Engineering & System Safety* 2014; 123: 137-44.
- [32] Echard B, Gayton N, Lemaire M, Relun N. A combined Importance Sampling and Kriging reliability method for small failure probabilities with time-demanding numerical models. *Reliability Engineering & System Safety* 2013; 111: 232-40.
- [33] Balesdent M, Morio J, Marzat J. Kriging-based adaptive Importance Sampling algorithms for rare event estimation. *Structural Safety* 2013; 44: 1-10.
- [34] Zhao H, Yue Z, Liu Y, Gao Z, et al. An efficient reliability method combining adaptive importance sampling and Kriging metamodel. *Applied Mathematical Modelling* 2015; 39: 1853-66.
- [35] Yun W, Lu Z, Jiang X. An efficient reliability analysis method combining adaptive Kriging and modified importance sampling for small failure probability. *Structural and Multidisciplinary Optimization* 2018; 58: 1383-93.
- [36] Sun Z, Wang J, Li R, Tong C. LIF: A new Kriging based learning function and its application to structural reliability analysis. *Reliability Engineering & System Safety* 2017; 157: 152-65.
- [37] Lelièvre N, Beaurepaire P, Mattrand C, Gayton N. AK-MCSi: A Kriging-based method to deal with small failure probabilities and time-consuming models. *Structural Safety* 2018; 73: 1-11.
- [38] Lv Z, Lu Z, Wang P. A new learning function for Kriging and its applications to solve reliability problems in engineering. *Computers & Mathematics with Applications* 2015; 70: 1182-97.
- [39] Zhang X, Wang L, Sørensen JD. REIF: A novel active-learning function toward adaptive Kriging surrogate models for structural reliability analysis. *Reliability Engineering & System Safety* 2019; 185: 440-54.
- [40] Yun W, Lu Z, Zhou Y, Jiang X. AK-SYSi: an improved adaptive Kriging model for system reliability

analysis with multiple failure modes by a refined U learning function. *Structural and Multidisciplinary Optimization* 2019; 59: 263-78.

- [41] Xiao N, Yuan K, Zhou C. Adaptive kriging-based efficient reliability method for structural systems with multiple failure modes and mixed variables. *Computer Methods in Applied Mechanics and Engineering* 2020; 359: 112649.
- [42] Zhou C, Xiao N, Li X, J Zhang. Structural reliability analysis using circular sampling surrogate models. *Journal of University of Electronic Science and Technology of China*. 2021; 50: 155-60 (in Chinese).
- [43] Wang D, Tan D, Liu L. Particle swarm optimization algorithm: an overview. *Soft Computing* 2018; 22: 387-408.
- [44] Gong Y, Li J, Zhou Y, Li Y, et al. Genetic Learning Particle Swarm Optimization. *IEEE Transactions On Cybernetics* 2016; 46: 2277-90.
- [45] Bichon BJ, Eldred MS, Swiler LP, Mahadevan S, et al. Efficient global reliability analysis for nonlinear implicit performance functions. *AIAA Journal* 2008; 46: 2459-68.
- [46] Eberhart R, Kennedy J. A new optimizer using particles swarm theory. In: *Proceedings of the Sixth international symposium on micro machine and human science*, Nagoya. 1995.
- [47] Perez RE, Behdinan K. Particle swarm approach for structural design optimization. *Computers & Structures* 2007; 85: 1579-88.
- [48] Luh G, Lin C, Lin Y. A binary particle swarm optimization for continuum structural topology optimization. *Applied Soft Computing* 2011; 11: 2833-44.
- [49] Elegbede C. Structural reliability assessment based on particles swarm optimization. *Structural Safety* 2005; 27: 171-86.
- [50] Yeh W, Lin Y, Chung YY, Chih M. A particle swarm optimization approach based on Monte Carlo Simulation for solving the complex network reliability problem. *IEEE Transactions On Reliability* 2010; 59: 212-21.
- [51] Bai B, Zhou C, Ye N. Application of multi-failure mode reliability-based particle swarm optimization algorithm. *Computers & Industrial Engineering* 2021; 161: 107627.
- [52] Clerc M, Kennedy J. The particle swarm - explosion, stability, and convergence in a multidimensional complex space. *IEEE Transactions On Evolutionary Computation* 2002; 6: 58-73.

- [53] Yi P, Wei K, Kong X, et al., Cumulative PSO-Kinging model for slope reliability analysis. Probabilistic Engineering Mechanics 2015; 39: 39-45.
- [54] Xu C, Chen W, Ma J, et al. AK-MSS: An adaptation of the AK-MCS method for small failure probabilities. Structural Safety 2020; 86: 101971.
- [55] Yun W, Lu Z, Jiang X, et al. AK-ARBIS: An improved AK-MCS based on the adaptive radial-based importance sampling for small failure probability. Structural Safety 2020; 82: 101891.
- [56] Liu Z, Lu Z, Ling C, et al. An improved AK-MCS for reliability analysis by an efficient and simple reduction strategy of candidate sample pool. Structures 2022; 35: 373-387.